INSTITUTE OF PHYSICS PUBLISHING JOURNAL OF PHYSICS: CONDENSED MATTER

J. Phys.: Condens. Matter **17** (2005) S3851–S3869 doi:10.1088/0953-8984/17/47/015

Velocity and processivity of helicase unwinding of double-stranded nucleic acids

M D Betterton[1] **and F Jülicher**[2]

[1] Department of Applied Mathematics, University of Colorado at Boulder, 526 UCB, Boulder, CO 80309, USA
[2] Max-Planck Institute for the Physics of Complex Systems, Nöthnitzerstraße 38, 01187 Dresden, Germany

Received 6 September 2005
Published 4 November 2005
Online at stacks.iop.org/JPhysCM/17/S3851

Abstract

Helicases are molecular motors which unwind double-stranded nucleic acids (dsNA) in cells. Many helicases move with directional bias on single-stranded (ss) nucleic acids, and couple their directional translocation to strand separation. A model of the coupling between translocation and unwinding uses an interaction potential to represent passive and active helicase mechanisms. A passive helicase must wait for thermal fluctuations to open dsNA base pairs before it can advance and inhibit NA closing. An active helicase directly destabilizes dsNA base pairs, accelerating the opening rate. Here we extend this model to include helicase unbinding from the nucleic-acid strand. The helicase processivity depends on the form of the interaction potential. A passive helicase has a mean attachment time which does not change between ss translocation and ds unwinding, while an active helicase in general shows a decrease in attachment time during unwinding relative to ss translocation. In addition, we describe how helicase unwinding velocity and processivity vary if the base-pair binding free energy is changed.

(Some figures in this article are in colour only in the electronic version)

1. Introduction

Helicases are motor proteins which separate the two strands of helical double-stranded nucleic acids (NA). Both DNA, RNA, and DNA–RNA hybrid helicases are found in cells. Strand separation requires breaking the base-pairing interactions between the two strands and therefore requires energy input. Unwinding is fuelled by NTP hydrolysis, typically of ATP. Helicases play a role in nearly every cellular process which involves NA, including DNA replication and repair, recombination, transcription, translation, and RNA processing [1]. Aberrant functioning of helicases is associated with genome instability (the accumulation of damage and errors in the genome), premature ageing, and cancer [2].

The essential common feature of all helicases is their ability to move along NA strands and couple motion to strand separation. (We use the terms opening, strand separation, and unwinding interchangeably.) For this reason, helicases are also NA translocases and share some features with other proteins which move on NA strands [3, 4].

The unwinding velocity and processivity of helicases are important for helicase function. The unwinding velocities of helicases range from tens to thousands of base pairs per second [1]. Helicase processivity is also variable. Processivity is most often defined as the average number of base pairs unwound per helicase binding event. Measured values of helicase processivity range from tens to tens of thousands of base pairs [1]. The processivity can be significantly altered by accessory proteins [5–7], polymerases [8], and multiple copies of the same helicase [9–11]. Attachment of an enzyme either to a surface or another protein tends to increase the processivity [12]. In single-molecule experiments on RecBCD helicase, a lower processivity was measured for a helicase that was free in solution [13] than for a helicase attached to the surface [14]. The velocity and processivity of helicase proteins are thought to be related to their biological roles. For example, replicative helicases are responsible for unwinding all cellular DNA during DNA replication. It has been proposed that replicative helicases should therefore have a high velocity and processivity, so that a small number of helicases can efficiently function in DNA copying. By contrast, a helicase which functions in DNA damage repair may only need to unwind a small region of DNA near a damage site; therefore, its velocity and processivity may be low. Understanding the physical basis of the velocity and processivity will help illuminate how these proteins may be optimized for different cellular roles.

Different definitions of processivity have been given in the literature. They include (i) the average time a motor stays attached to its track, (ii) the average number of steps a motor travels before detaching, (iii) the number of ATP molecules hydrolysed before the motor falls off the track, and (iv) the probability that a motor takes one more step (as opposed to unbinding before the next step). For helicases and other motors which interact with obstacles, this picture is complicated. We may consider both the *translocation processivity*, which is the average number of forward steps taken by the helicase during one binding event, and the *unwinding processivity*, which is the average number of NA base pairs (bp) unwound during a helicase binding event. The translocation and unwinding processivity are not equivalent, and their values vary with initial conditions. Unwinding processivity is usually measured for helicases; however, the measured value can depend on where the motor binds relative to where it begins unwinding the NA.

Because helicase proteins are involved in a wide range of cellular processes, many different types of helicase protein are found in cells. Even the relatively simple bacterium *E. coli* has at least 11 different types of helicase. Helicases are structurally diverse, and not all helicases share a common mechanism. However, many helicases share the ability to translocate directionally on single-stranded (ss) NA, especially members of superfamilies I and II [4]. Motion on ssNA is analogous to the motion of a classical motor protein which moves with directional bias on an infinite, one-dimensional lattice (figure 1). Single-stranded NA is polar, with one end labelled the $3'$ end and the other the $5'$ end. Helicases which directionally translocate on ssNA are referred to as $3' \rightarrow 5'$ helicases or $5' \rightarrow 3'$ helicases, depending on which direction they move on the single strand. When the helicase is near the ss–double-strand (ds) junction, the helicase can move the junction forward, creating additional ssNA 'track' as it moves.

A natural question in the study of helicases is how a protein may efficiently couple translocation to unwinding. In the biochemical literature on helicases, this coupling is classified as passive or active [15, 1, 3, 4]. A passive helicase waits for a thermal fluctuation that opens part of the dsNA, and then moves forward, binds to the newly available ssNA, and prevents the

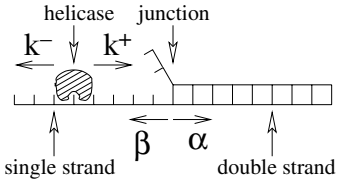

Figure 1. Sketch of helicase on a nucleic acid strand. The helicase moves forward—toward the junction where the dsNA strand opens—at rate k^+ and backward at rate k^-. The NA opens at rate α and closes at rate β.

NA from closing. An active helicase directly destabilizes the dsNA, presumably by changing the free energy of the ds state.

Many different types of helicase have been studied experimentally in some detail [1, 3, 16]. In recent years, single-molecule experiments have been performed for several helicases, directly measuring helicase unwinding rates. The helicase RecBCD, which is also an exonuclease (it degrades one of the unwound strands as it moves), has been studied by several groups [17, 13, 18, 14, 19]. Interpretation of the RecBCD data is complicated by the fact that RecBCD contains two helicases of opposite polarity, which move on both strands of the DNA [20–22]. Bulk kinetic experiments on RecBCD have tried to determine the kinetic step size by fitting the data to a model of helicase unwinding [23–26]; to date, physical steps of this helicase have not been directly observed. Single-strand translocation and double-strand unwinding were observed for Rep helicase using single-molecule FRET [27, 28]. The motion of the RNA helicase DbpA has been observed with AFM [29]. Single-molecule experiments on UvrD helicase have observed unwinding, and evidence of strand-switching [30]. Finally, single-molecule FRET has been used to study the T4 replisome, the replication machinery which includes the T4 helicase [31].

Although extensive biochemical and structural studies of helicases have been performed, few descriptions of the physics of helicase unwinding exist. Previous work includes a 'flashing field' model specific to hexameric ring helicases [32], a description of a helicase as a biased random walk, which considered how the density of histones affects the random walk [33], and a model where helicase motion is represented as a propagating front [34, 35]. Molecular dynamics simulations have addressed properties of PcrA helicase [36]. Recent work includes a proposal that HCV helicase functions by a ratchet mechanism [37], a theory for two coupled motor proteins, proposed to describe RecBCD helicase [38], and a detailed description of the mechanochemistry of T7 helicase [39]. A physical description of helicase unwinding of NA has been proposed which contains both active and passive opening as different cases in a general framework [40, 41]. Here we extend the description of helicase unwinding to allow calculation of helicase processivity.

We represent a helicase by a particle which moves with directional bias on a one-dimensional lattice (corresponding to the ssNA). The ss–ds junction represents an obstacle on the lattice which blocks the helicase motion while also moving due to thermal fluctuations. Our model describes different forms of the interaction between the particle and the mobile obstacle. This scenario—a moving particle which interacts with an obstacle—also exists in other biological systems. Peskin, Odell, and Oster introduced the 'polymerization ratchet' to describe how a growing biological polymer can exert a force against a fluctuating obstacle [42]. They argued that the rate of polymerization is limited by the time required for the obstacle to diffuse one monomer size. In the language of our model, described below, this scenario corresponds to a hard-wall interaction potential between the growing tip and the obstacle.

As we show here, other forms of interaction can show significantly different velocity and processivity. Another example of the interaction of a motor with a second degree of freedom is the kinesin-family motor protein MCAK, which induces microtubule depolymerization if it interacts with the microtubule end [43–45]. This process is relevant in the generation of force during the separation of chromosomes by the mitotic spindle. Finally, the interaction of two motor proteins on a filament is another example for which our approach is relevant.

In this paper, we first review a simple description which captures both active and passive unwinding by helicases [40, 41]. This framework considers a single helicase which does not unbind from the NA strand, and permits us to calculate the unwinding velocity for a given interaction potential (section 2). The unwinding velocity for a passive helicase with hard-wall interaction potential is typically significantly slower than the ss translocation rate of the motor far from the ss–ds junction. For a simple form of active opening, the velocity approaches the single-strand translocation rate of the motor. In other words, an optimized active helicase can unwind NA as fast as it translocates on ssNA. Comparable rates of ss translocation and unwinding are therefore a signature of active opening.

We then extend this description to include a nonzero unbinding rate, and develop a simple model of unbinding that captures the key effects. We assume that the unbinding rate may be different for a helicase translocating on ssNA than for a helicase unwinding dsNA, because the interaction potential alters the unbinding rate when the helicase is near the ss–ds junction. If the interaction free energy is larger, then the helicase will unbind more quickly. In particular, we assume that the free-energy difference between the bound state and the barrier to unbinding is decreased by the amount of the interaction potential. We assume that the unbinding rate is independent of the helicase biochemical state. The unbinding rate is determined only by the height of the energy barrier separating the bound from the unbound states.

This model of unbinding allows us to calculate different measures of processivity (section 3). We discuss the dependence of the processivity on the shape of the interaction potential. The average attachment time of a helicase is particularly simple for a passive helicase: the helicase unbinding rate during unwinding is equal to the unbinding rate during ss translocation (section 4). By contrast, the helicase attachment time is lower during unwinding than during ss translocation for an active helicase (section 5). Decreased attachment time during unwinding is a signature of active unwinding.

Finally, in our conclusion, we discuss the connection between our results and experiments (section 6).

2. Active and passive unwinding

In our simplified discrete description of helicase unwinding, the position of the motor—the helicase—along its track is labelled by the integer n, and the position of the obstacle—the ss–ds junction—is denoted m (figure 1). The motor is assumed to move toward increasing n, and we expect $n \leqslant m$. The interaction between motor and obstacle is characterized by an interaction energy $U(m-n)$ which depends only on the obstacle–motor separation. We assume $U \to 0$ for $m \gg n$ and $U \to \infty$ for $m < n$.

One simple form of this potential is a hard-wall interaction of zero range: $U = 0$ for $m > n$ and $U = \infty$ for $m \leqslant n$. For a hard-wall potential, a motor which is near the obstacle ($n = m - 1$) can advance only if the obstacle undergoes a fluctuation which increases m. This situation corresponds to passive unwinding. For active unwinding, the interaction between the motor and obstacle has nonzero range: when the helicase is near the ss–ds junction, both the kinetics of NA opening and the helicase motion are altered by the interaction. We will discuss interaction potentials which represent active unwinding below.

We denote the rates of forward and backward hopping of the motor on the lattice far from the obstacle by k^+ and k^-. The hopping rates for forward and backward motion of the junction (corresponding to the opening and closing of dsNA) in the absence of the helicase are denoted α and β. The ratio of these rates is given by $\alpha/\beta = \mathrm{e}^{-\Delta G}$, where ΔG is the free energy difference per base between dsNA and two complementary ssNA strands. (Note that we use units where $k_\mathrm{B}T = 1$.) This energy difference is positive when dsNA is thermodynamically stable. For simplicity, we write a similar expression for the ratio of forward and backward hopping rates of the helicase, $k^+/k^- = \mathrm{e}^{\Delta\mu}$. Here $\Delta\mu$ denotes the chemical free energy of ATP hydrolysis which drives helicase motion. This expression applies when each hydrolysis event is tightly coupled to a forward step on the NA. We use this simplification here to discuss principles which do not depend on the validity of this assumption. Note that an effective value of $\Delta\mu$ can be derived in certain limits from a more detailed description of the mechanochemical coupling [41].

The interaction between the helicase and the ss–ds junction modifies the hopping rates. We express the ratios of these rates as

$$\frac{\beta_j}{\alpha_{j-1}} = \frac{\beta}{\alpha}\mathrm{e}^{-[U(j-1)-U(j)]}, \tag{1a}$$

$$\frac{k_j^+}{k_{j-1}^-} = \frac{k^+}{k^-}\mathrm{e}^{-[U(j-1)-U(j)]}, \tag{1b}$$

where α_j, β_j, k_j^+ and k_j^- are the position-dependent rates when the helicase and the junction are separated by $j = m - n$ bases. To fully specify the position-dependent rates we write

$$k_j^+ = k^+\mathrm{e}^{-f[U(j-1)-U(j)]}, \tag{2a}$$

$$k_{j-1}^- = k^-\mathrm{e}^{-(f-1)[U(j-1)-U(j)]}, \tag{2b}$$

$$\beta_j = \beta\mathrm{e}^{-f[U(j-1)-U(j)]}, \tag{2c}$$

$$\alpha_{j-1} = \alpha\mathrm{e}^{-(f-1)[U(j-1)-U(j)]}, \tag{2d}$$

where the parameter f describes the energy barrier of the transitions. For a one-dimensional reaction, f corresponds to the fractional distance of the peak of the barrier between the two adjacent states and thus $0 < f < 1$.

For the simple case of a hard-wall potential (figure 2(a)), the helicase prevents NA closing when $j = 1$. Therefore $\beta_1 = 0$ because $U(0)$ is infinite. Infinite $U(0)$ also implies $k_1^+ = 0$: the helicase must wait until a thermal fluctuation opens the NA before advancing. An interaction potential with nonzero range corresponds to enzymatically assisted opening. For simplicity, we use a linear potential with range N and slope U_0. The discretized potential is shown in figures 2(b) and (c). The potential energy increases in N steps, each of energy U_0, before a hard-wall is reached. The increase in energy due to this potential facilitates opening of the dsNA: $U(j-1) > U(j)$ implies $\beta_j/\alpha_{j-1} < \beta/\alpha$. In addition, the interaction energy slows helicase forward motion. We assume $U \to 0$ for $j \to \infty$, so that no interaction occurs for large separations.

The probability $P(j, l, t)$ that the helicase and junction are at separation j and midpoint position $l = m + n$ satisfies the master equation

$$\begin{aligned}\frac{\mathrm{d}P(j,l,t)}{\mathrm{d}t} &= -(\alpha_j + \beta_j + k_j^+ + k_j^-)P(j,l) + \alpha_{j-1}P(j-1,l-1) \\ &\quad + \beta_{j+1}P(j+1,l+1) + k_{j+1}^+P(j+1,l-1) + k_{j-1}^-P(j-1,l+1).\end{aligned} \tag{3}$$

Since the rates depend only on j, we define the distribution $\mathcal{P}_j = \sum_l P(j,l,t)$. After a relaxation time which depends on the rates α, β, k^+, and k^-, the distribution $\mathcal{P}_j$ relaxes to a

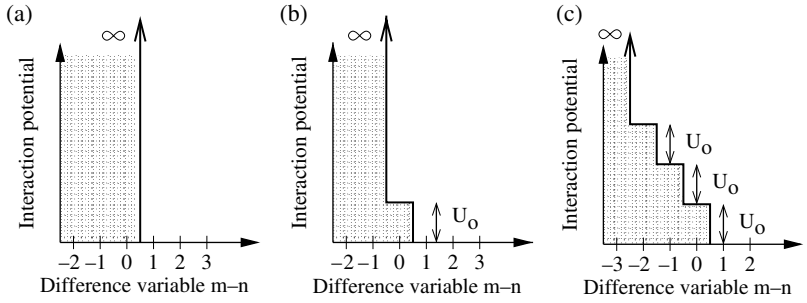

Figure 2. Interaction energies between the helicase and ss–ds junction as a function of their distance $m - n$ in number of bases. (a) Hard-wall potential. (b) Potential with a single step. (c) Potential with three steps.

stationary state which satisfies the recursion relation

$$\mathcal{P}_{j+1} = \frac{k_j^- + \alpha_j}{k_{j+1}^+ + \beta_{j+1}} \mathcal{P}_j. \tag{4}$$

This steady-state distribution can be used to calculate the mean velocity (bp s^{-1}) [40, 41]

$$v = \tfrac{1}{2} \sum_j (k_j^+ + \alpha_j - k_j^- - \beta_j) \mathcal{P}_j. \tag{5}$$

This expression for v has a simple physical interpretation—the quantity in parentheses is the unwinding rate at separation j, which is multiplied by the probability $\mathcal{P}_j$ of finding the complex at separation j. The effective diffusion coefficient which characterizes velocity fluctuations is

$$D = \tfrac{1}{4} \sum_j (k_j^+ + \alpha_j + k_j^- + \beta_j) \mathcal{P}_j. \tag{6}$$

We assume that the helicase remains bound to the NA for all time. Therefore the expressions for v and D are true steady-state values reached by a real system in the long-time limit. In the results below, unwinding velocities of a bound helicase are calculated under this steady-state assumption.

3. Processive and unprocessive unwinding

In section 2 we assumed that the motor never unbinds from the track, so the model represents a motor which is infinitely processive. Real motors have finite processivity—they unbind eventually. This effect can be incorporated in our description by introducing the rate of unbinding γ. We assume that γ depends on the separation j between motor and obstacle, but has no other position or time dependence. For a repulsive potential such as the linear potential discussed above, when the motor and obstacle are close to each other the free energy of motor and junction is increased. This typically leads to an increased rate of unbinding. This effect can be described by writing [46]

$$\gamma_j = \gamma e^{U(j)}. \tag{7}$$

Here $\gamma > 0$ is the detachment rate for motion on a single strand far from the junction.

The time evolution of the probability distribution is then described by

$$\frac{\mathrm{d}P(j,l)}{\mathrm{d}t} = -(k_j^+ + k_j^- + \alpha_j + \beta_j + \gamma_j)P(j,l) + \alpha_{j-1}P(j-1,l-1) + \beta_{j+1}P(j+1,l+1) + k_{j+1}^+P(j+1,l-1) + k_{j-1}^-P(j-1,l+1). \tag{8}$$

Note that this expression differs from equation (3) only in the additional term proportional to the unbinding rate γ_j. The other rates are unchanged as defined above, in equation (2). We assume that at time $t = 0$ the helicase and junction have a specific position determined by $j = j_0$ and $l = l_0$. Therefore,

$$P(j,l,t=0) = \delta_{jj_0}\delta_{ll_0}, \tag{9}$$

where $\delta_{jk} = 1$ for $j = k$ and 0 otherwise.

3.1. Processivity and attachment time

We characterize the processivity by the average attachment time $\langle\tau\rangle$ of the motor and by both the *translocation processivity* $\langle\delta n\rangle$, which is the average number of forward steps taken by the helicase during one binding event, and the *unwinding processivity* $\langle\delta m\rangle$, which is the average number of NA bp unwound during one helicase binding event. These measures of processivity depend on initial conditions. If the helicase binds near the ss–ds junction, then the translocation and unwinding processivities are similar. However, if the helicase binds to a ss region far from the junction, then the unwinding processivity can be much smaller than the translocation processivity. If the NA can close on average under these conditions, the corresponding unwinding processivity becomes negative.

The mean attachment time is defined as

$$\langle\tau\rangle = \int_0^\infty \mathrm{d}t\, t \sum_{j,l} \gamma_j P(j,l,t). \tag{10}$$

Similarly, the translocation and unwinding processivities can be defined by

$$\langle\delta n\rangle = \frac{\langle\delta l\rangle - \langle\delta j\rangle}{2}, \tag{11}$$

$$\langle\delta m\rangle = \frac{\langle\delta l\rangle + \langle\delta j\rangle}{2}. \tag{12}$$

Here, the average changes in j and l during unwinding are

$$\langle\delta j\rangle = \int_0^\infty \mathrm{d}t \sum_{j,l} (j - j_0)\gamma_j P(j,l,t), \tag{13}$$

$$\langle\delta l\rangle = \int_0^\infty \mathrm{d}t \sum_{j,l} (l - l_0)\gamma_j P(j,l,t). \tag{14}$$

The translocation processivity $\langle\delta n\rangle = \langle n - n_0\rangle$ is the mean number of steps the motor takes in one direction before detaching and the unwinding processivity $\langle\delta m\rangle = \langle m - m_0\rangle$ is the mean number of steps the obstacle moves per binding event. The above expressions can be simplified using Laplace transforms [46]. The Laplace transform of $P(j,l,t)$ is

$$\tilde{P}_{j,l}(s) = \int_0^\infty \mathrm{d}t\, \mathrm{e}^{-st} P(j,l,t). \tag{15}$$

Summing equation (8) over j and l, we obtain

$$\sum_{j,l} \frac{\mathrm{d}P(j,l,t)}{\mathrm{d}t} = \sum_{j,l} -\gamma_j P(j,l,t). \tag{16}$$

We can thus simplify the expression for $\langle\tau\rangle$ in equation (10) by integrating by parts:

$$\langle\tau\rangle = -\sum_{j,l}\int_0^\infty \mathrm{d}t\, t\frac{\mathrm{d}P(j,l,t)}{\mathrm{d}t},$$
$$= \sum_{j,l}\int_0^\infty \mathrm{d}t\, P(j,l,t). \tag{17}$$

The boundary terms vanish because at the lower boundary $t = 0$, while for long times the probability approaches zero at all sites because the motor unbinds.

Defining the coefficients

$$Q_{j,l} = \tilde{P}_{j,l}(s=0) = \int_0^\infty \mathrm{d}t\, P(j,l,t), \tag{18}$$

the average attachment time can be expressed as

$$\langle\tau\rangle = \sum_{j,l} Q_{j,l}. \tag{19}$$

Similarly, the j and l processivities are given by

$$\langle\delta j\rangle = \int_0^\infty \mathrm{d}t\, \sum_{j,l}(j-j_0)\gamma_j P(j,l,t), \tag{20}$$
$$= \sum_{j,l}(j-j_0)\gamma_j Q_{j,l}, \tag{21}$$

and

$$\langle\delta l\rangle = \sum_{j,l}(l-l_0)\gamma_j Q_{j,l}. \tag{22}$$

We therefore need to calculate $Q_{j,l}$, the Laplace-transformed probability at $s = 0$, to obtain the average attachment time and the mean change in j and l during a single binding event. The translocation and unwinding processivities are obtained by equations (11) and (12).

The coefficients $Q_{j,l}$ are obtained by solving the Laplace transform of equation (8) for $s = 0$:

$$\int_0^\infty \mathrm{d}t\, \mathrm{e}^{-st}\frac{\mathrm{d}P(j,l)}{\mathrm{d}t} = -(k_j^+ + k_j^- + \alpha_j + \beta_j + \gamma_j)\tilde{P}_{j,l}(s) + \alpha_{j-1}\tilde{P}_{j-1,l-1}(s) + \beta_{j+1}\tilde{P}_{j+1,l+1}(s)$$
$$+ k_{j+1}^+\tilde{P}_{j+1,l-1}(s) + k_{j-1}^-\tilde{P}_{j-1,l+1}(s). \tag{23}$$

Note that the rates have no explicit time dependence. As above, integrating by parts leads to

$$\int_0^\infty \mathrm{d}t\, \mathrm{e}^{-st}\,\frac{\mathrm{d}P(j,l)}{\mathrm{d}t} = P(j,l,t)\mathrm{e}^{-st}\big|_0^\infty + s\int_0^\infty \mathrm{d}t\, \mathrm{e}^{-st}P(j,l,t),$$
$$= -P(j,l,t=0) + s\tilde{P}_{j,l}(s),$$
$$= -\delta_{jj_0}\delta_{ll_0} + s\tilde{P}_{j,l}(s). \tag{24}$$

Here we have used the initial condition, equation (9). Thus the Laplace-transformed equations are

$$-\delta_{jj_0}\delta_{ll_0} + s\tilde{P}_{j,l}(s) = -(k_j^+ + k_j^- + \alpha_j + \beta_j + \gamma_j)\tilde{P}_{j,l}(s) + \alpha_{j-1}\tilde{P}_{j-1,l-1}(s) + \beta_{j+1}\tilde{P}_{j+1,l+1}(s)$$
$$+ k_{j+1}^+\tilde{P}_{j+1,l-1}(s) + k_{j-1}^-\tilde{P}_{j-1,l+1}(s). \tag{25}$$

In general, these equations could be solved for arbitrary s. We only require the Laplace-transformed probability evaluated at $s = 0$. The coefficients $Q_{j,l}$ satisfy the equation

$$\delta_{jj_0}\delta_{ll_0} = (k_j^+ + k_j^- + \alpha_j + \beta_j + \gamma_j)Q_{j,l} - \alpha_{j-1}Q_{j-1,l-1} - \beta_{j+1}Q_{j+1,l+1}$$
$$- k_{j+1}^+Q_{j+1,l-1} - k_{j-1}^-Q_{j-1,l+1}. \tag{26}$$

These equations describe a discrete drift-plus-diffusion system in two dimensions with an inhomogeneous term.

Equation (26) can be solved by a product ansatz

$$Q_{j,l} = R_j T_l. \tag{27}$$

Using this ansatz in equation (26), and choosing the normalization $\sum_l T_l = 1$ and $\sum_j \gamma_j R_j = 1$, the coefficients R_j satisfy

$$-\delta_{jj_0} = -(k_j^+ + k_j^- + \alpha_j + \beta_j + \gamma_j)R_j + (\alpha_{j-1} + k_{j-1}^-)R_{j-1} + (\beta_{j+1} + k_{j+1}^+)R_{j+1}. \tag{28}$$

The coefficients T_l satisfy the equation

$$\delta_{ll_0} = (p + q + 1)T_l - pT_{l-1} - qT_{l+1}. \tag{29}$$

Here we have defined

$$p = \sum_j (\alpha_j + k_j^+)R_j, \tag{30}$$

$$q = \sum_j (\beta_j + k_j^-)R_j. \tag{31}$$

3.2. *Simplified expressions for processivity*

The average attachment time $\langle\tau\rangle$ and the quantities $\langle\delta j\rangle$ and $\langle\delta l\rangle$ can be expressed in terms of the R_j and T_l:

$$\langle\tau\rangle = \sum_j R_j, \tag{32}$$

$$\langle\delta j\rangle = \sum_j (j - j_0)\gamma_j R_j, \tag{33}$$

$$\langle\delta l\rangle = \sum_l (l - l_0)T_l. \tag{34}$$

The solutions to equation (28) depend on the shape of the interaction potential. Some examples are discussed below. However, in general equation (29) can be solved formally. Equation (29) is a second-order, linear, inhomogeneous difference equation. Since we have assumed translational invariance in l, the resulting solution is independent of l_0. Therefore we choose $l_0 = 0$ for convenience. The solutions have the form $T_l = y^l$ for $l \neq 0$. Using this ansatz, y obeys a quadratic equation

$$y^2 - (1 + a)y + (a - b) = 0, \tag{35}$$

where $a = (1 + p)/q$ and $b = 1/q$. We denote by y_+ and y_- the positive and negative roots of equation (35). For $l \geqslant 0$, $T_l = A' y_-^l$, while for $l \leqslant 0$ the solution is $T_l = A y_+^l$, since T_l must vanish for $l \to \pm\infty$. Requiring that T_0 is the same for both expressions implies $A = A'$. Finally, equation (29) for $l = 0$ leads to

$$A = b\left(1 + a - y_- - \frac{a - b}{y_+}\right)^{-1}. \tag{36}$$

Formally, we can use equation (34) to determine $\langle\delta l\rangle$:

$$\langle\delta l\rangle = \sum_l l T_l, \tag{37}$$

$$= A\sum_{l=1}^{\infty}\left(l y_-^l - l y_+^{-l}\right), \tag{38}$$

$$= A\left[\frac{y_-}{(1 - y_-)^2} - \frac{y_+}{(1 - y_+)^2}\right]. \tag{39}$$

Note, however, that A and $y_\pm$ depend on the shape of the interaction potential via the coefficients R_j. Once these coefficients have been determined, the quantities $\langle\tau\rangle$, $\langle\delta j\rangle$, and $\langle\delta l\rangle$, and therefore $\langle\delta n\rangle$ and $\langle\delta m\rangle$, can easily be obtained.

4. Velocity and processivity for a hard-wall interaction potential

4.1. Velocity

For the hard-wall potential, the unwinding velocity is given by

$$v_{\mathrm{HW}} = \frac{\alpha k^+ - \beta k^-}{\beta + k^+}. \tag{40}$$

The velocity is positive whenever $k^+/k^- > \beta/\alpha$, that is, the free energy change ΔG which drives NA closing must be smaller than the chemical potential $\Delta\mu$ of ATP hydrolysis. The maximum v_{HW} occurs for a unidirectional helicase ($k^- = 0$). This upper bound is

$$v_{\mathrm{HW}}^{\max} = \frac{\alpha}{\beta}\left(\frac{k^+}{1 + k^+/\beta}\right) \approx \frac{\alpha}{\beta}k^+, \tag{41}$$

where the approximation holds if $k^+ \ll \beta$. Thus a passive helicase unwinds more slowly than it translocates on ssNA by a factor $\approx\alpha/\beta$. This result has a simple interpretation: the base pair adjacent to the helicase has a probability α/β of being open. Thus, when the helicase attempts a forward hop it succeeds with probability α/β.

4.2. Processivity

For a hard-wall potential, the average attachment time, translocation processivity, and unwinding processivity can be calculated analytically. We solve equation (28) for R_j for the simple case $j_0 = 1$. For $j > 1$, the rates are independent of j and we have

$$R_{j+1} = (1 + d)R_j + (d - e)R_{j-1}, \tag{42}$$

where we have defined

$$d = \frac{\alpha + k^- + \gamma}{\beta + k^+}, \tag{43}$$

$$e = \frac{\gamma}{\beta + k^+}. \tag{44}$$

This equation has solutions of the form $R_j = x_\pm^j$, where the $x_\pm$ are the positive and negative root of the quadratic equation $x^2 - (1+d)x + (e-d) = 0$. The boundary condition that R_j vanishes for large j imposes $R_j = Bx_-^j$. From equation (28) at $j = 1$, we find $(\beta+k^+)(R_2 - dR_1) = -1$ and

$$B = [x_-(\beta + k^+)(d - x_-)]^{-1}. \tag{45}$$

With these expressions, $\langle\tau\rangle = \gamma^{-1}$. This simple result follows since for the hard-wall case $\gamma_j = \gamma$ is independent of the separation j.

The average change in j is

$$\langle\delta j\rangle = \frac{x_-}{1 - x_-}. \tag{46}$$

To determine $\langle\delta l\rangle$, we note that for the hard-wall case

$$p = \gamma^{-1}(\alpha + k^+ x_-), \tag{47}$$

$$q = \gamma^{-1}(k^- + \beta x_-). \tag{48}$$

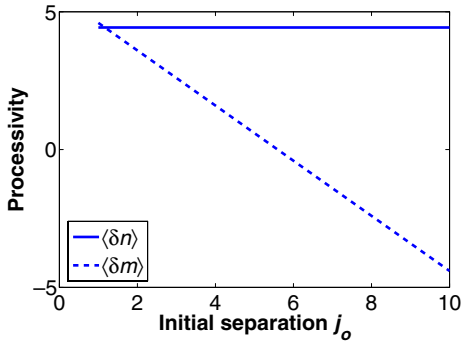

Figure 3. The translocation processivity $\langle \delta n \rangle$ and unwinding processivity $\langle \delta m \rangle$ as a function of the initial separation j_0 between motor and junction. When $j_0 = 1$, the translocation and unwinding processivities are approximately equal. As the separation j_0 increases, the translocation processivity $\langle \delta n \rangle$ is approximately constant, while the unwinding processivity $\langle \delta m \rangle$ decreases. The parameters are $\alpha = 10^5\ \mathrm{s}^{-1}$, $\beta = 7 \times 10^5\ \mathrm{s}^{-1}$, $k^+ = 1$ base s^{-1}, $k^- = 0.01$ base s^{-1}, and $\gamma = 0.03\ \mathrm{s}^{-1}$. Calculations were done numerically using a grid size of $M = 100$ in j.

The quantity $\langle \delta l \rangle$ now follows from equation (39). In the hard-wall case, the translocation processivity is approximately the unwinding velocity times the attachment time: $\langle \delta m \rangle \approx v \langle \tau \rangle$, as we would expect for position-independent detachment. Note that this result depends on initial conditions and is valid for $j_0 = 1$.

When $j_0 = 1$, the translocation and unwinding processivities are approximately equal. As the separation between the motor and obstacle increases, the unwinding processivity drops. A negative unwinding processivity reflects net backwards motion of the obstacle while the motor is bound. For a large separation between the motor and obstacle, they have no effect on each other. In figure 3, the processivities are shown as a function of j_0 with other parameters fixed.

The helicase adjacent to the junction can only move when the junction opens. Therefore, the velocity and the processivities depend strongly on the base pair binding free energy ΔG. The velocity and the measures of processivity are displayed in figure 4 as a function of ΔG. In this calculation, we assume that β is constant and $\alpha = \beta \mathrm{e}^{-\Delta G}$. The value $\Delta G = 2$ corresponds to the sequence averaged value for typical genomic DNA. For small ΔG, the processivity increases dramatically, because the binding energy driving NA closing is decreased.

5. Velocity and processivity of an active helicase

5.1. Velocity

Active opening can be represented by an interaction potential with nonzero range between junction and helicase. For simplicity, we choose linear potentials characterized by a range of N steps and a step height U_0 (figure 2). The repulsive interaction between helicase and junction implies that for small separation j within the range of the potential the rates of junction opening and helicase backward hopping are increased. The unwinding velocity for such a potential, relative to the hard-wall case, is [40, 41]

$$\frac{v_N}{v_{\mathrm{HW}}} = \frac{c^N(\mathrm{e}^{-U_0} - c) + (1-c)\mathrm{e}^{-fU_0}(\mathrm{e}^{-NU_0} - c^N)}{c^N(\mathrm{e}^{-U_0} - c) + (1-c)\mathrm{e}^{-U_0}(\mathrm{e}^{-NU_0} - c^N)}. \tag{49}$$

Note that the helicase cannot increase the unwinding rate beyond a certain limit. Assuming $0 < f < 1$, the unwinding rate has an upper bound $v_N \leqslant c^{-1} v_{\mathrm{HW}}$, where $c = (\alpha + k^-)/(\beta + k^+)$.

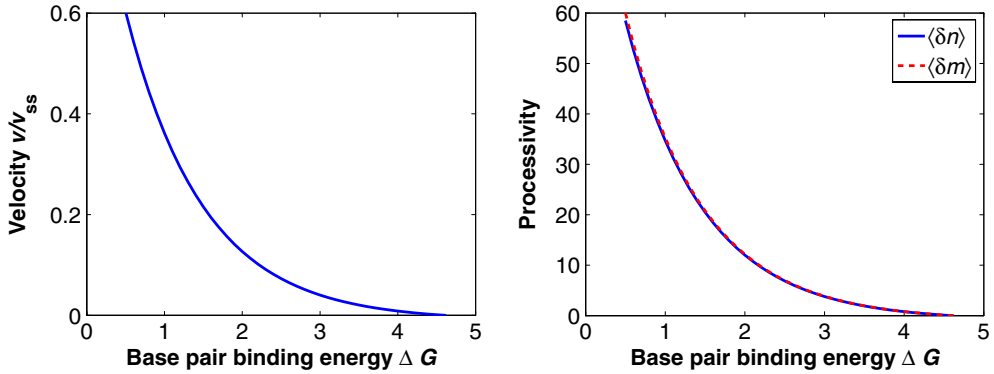

Figure 4. Velocity and processivity as a function of the base-pairing energy ΔG for a hard-wall potential. We varied the opening rate of the ss–ds junction, assuming that the closing rate is constant. Therefore $\alpha = \beta e^{-\Delta G}$. Left, unwinding rate v_{HW}/v_{ss} as a function of ΔG. Right, translocation and unwinding processivity as a function of ΔG. Parameters are $\beta = 7 \times 10^5$ s^{-1}, $k^+ = 1$ base s^{-1}, $k^- = 0.01$ base s^{-1}, $\gamma = 0.01$ s^{-1}, and $j_0 = 1$.

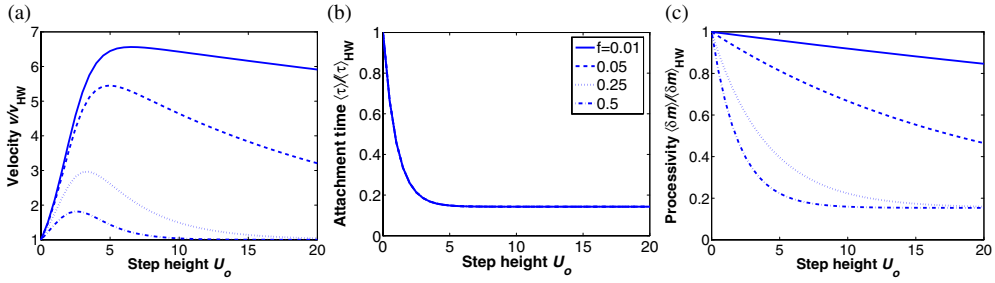

Figure 5. Variation of unwinding velocity, average attachment time, and unwinding processivity as a function of step height for a one-step potential. The parameters are $\alpha = 10^5$ s^{-1}, $\beta = 7 \times 10^5$ s^{-1}, $k^+ = 1$ base s^{-1}, $k^- = 0.01$ base s^{-1}, and, for the processivity calculation, $\gamma = 0.01$ s^{-1}, $j_0 = 1$, and grid size $M = 100$.

The unwinding velocity for one step ($N = 1$) is displayed in figure 5(a) as a function of the step height U_0 for different values of the parameter f. For small U_0, the unwinding rate increases with increasing step height U_0 because the presence of the step facilitates NA opening. For large step heights, the unwinding rate decreases, because the repulsive potential reduces the rate of helicase forward motion. The unwinding velocity for different values of N is shown in figure 6(a) as a function of U_0. For increasing N, the opening rate becomes more sensitive to U_0 and the maximum occurs at higher values. For large N, the maximum unwinding rate occurs for $U_* \approx -\ln c \approx \Delta G$. In this case fastest unwinding occurs when the slope of the potential matches the base-pairing energy of the NA.

5.2. *Processivity for active unwinding*

Active unwinding results in a decrease of the mean attachment time, as compared to ss translocation or passive opening for which $\langle\tau\rangle = \gamma^{-1}$. This is a consequence of the repulsive interaction potential which leads to increased unbinding rate for small j. The dependence of the average attachment time on the step height is displayed in figure 5(b) for $N = 1$. For a potential with one step, $\langle\tau\rangle$ decreases rapidly with step height to a plateau value $\approx 0.2\gamma^{-1}$.

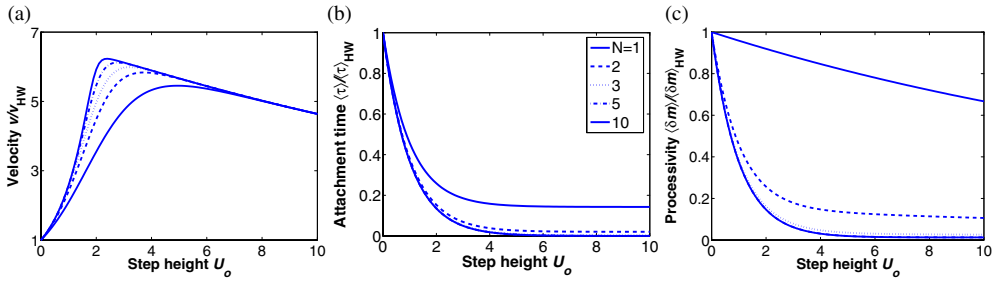

Figure 6. Variation of velocity, average attachment time, and unwinding processivity with step height, for potentials with varying numbers of steps. The parameters are $f = 0.05$, $\alpha = 10^5$ s^{-1}, $\beta = 7 \times 10^5$ s^{-1}, $k^+ = 1$ base s^{-1}, $k^- = 0.01$ base s^{-1}, and, for the processivity calculation, $\gamma = 0.01$ s^{-1}, $j_0 = 1$, and $M = 100$.

This decrease is independent of f, since the unbinding rate does not depend on the barrier between states of different j. Note that the limits $U_0 \to 0$ and $U_0 \to \infty$ do not give the same result for the processivity because the initial conditions are different: $U_0 \to 0$ corresponds to a hard-wall potential with $j_0 = 1$, while $U_0 \to \infty$ corresponds to a hard-wall potential but with $j_0 = 0$.

The decrease of $\langle\tau\rangle$ for increasing U_0 is similar but even more pronounced for potentials with longer range, as shown in figure 6(b). For $N \geqslant 2$, the average attachment time rapidly decreases to $< 0.01\gamma^{-1}$. Decreased attachment time during unwinding (as compared to ss translocation) is a strong signature of active unwinding.

Because the attachment time decreases with increasing step height, the translocation and unwinding processivities also tend to decrease. However, for a one-step potential $\langle\delta n\rangle$ and $\langle\delta m\rangle$ decrease slowly for increasing step height when f is small (figure 5(c)). This occurs because the rapid increase in the velocity approximately cancels the decrease in attachment time, leading to a processivity that is relatively insensitive to step height. For larger numbers of steps, a decrease in $\langle\delta m\rangle$ occurs as U_0 increases (figure 6(c)). These curves are approximately exponentially decreasing functions, with a decay constant determined by f. Small f means that the processivity varies slowly in the biologically plausible range between 0 and 20 k_BT. Note that above $U_0 = 20$ little or no increase in the velocity can be achieved by increasing the step size.

5.3. Dependence on base-pair binding energy

The velocity and attachment time are sensitive to the mean free energy per base pair ΔG. We assume that the rate β is constant and $\alpha = \beta e^{-\Delta G}$. For simplicity, we show results only for a potential with $N = 1$. The dependence of v and $\langle\tau\rangle$ on ΔG depends on the step height U_0. For a hard-wall potential, the velocity varies exponentially as a function of ΔG. As U_0 increases, the velocity becomes less sensitive to ΔG (figure 7(a)). Thus for $U_0 = 5$ the displayed curve decreases slowly with increasing ΔG. The attachment time $\langle\tau\rangle$ shows the opposite trend: for a hard-wall interaction potential, the attachment time is independent of ΔG. The attachment time is also weakly dependent on ΔG for small U_0, while for larger U_0, $\langle\tau\rangle$ varies more rapidly (figure 7(b)). The processivity $\langle\delta m\rangle$ as a function of ΔG exhibits the same behaviour independent of U_0 (figure 7(c)), because the variation in velocity and attachment time as a function of step height approximately cancel. Therefore, measurements of velocity and attachment time have greater power to elucidate aspects of the potential.

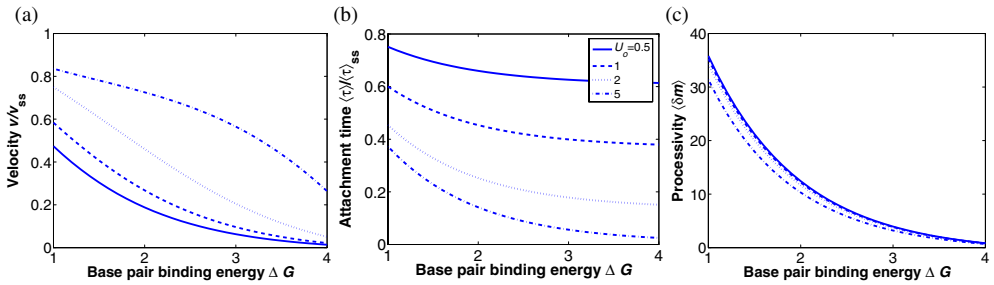

Figure 7. Unwinding velocity, attachment time, and unwinding processivity versus free-energy per base pair for a one-step potential. We fix the closing rate and therefore $\alpha = \beta e^{-\Delta G}$. The parameters are $f = 0.05$, $\beta = 7 \times 10^5$ s^{-1}, $k^+ = 1$ base s^{-1}, $k^- = 0.01$ base s^{-1}, and, for the processivity curves, $\gamma = 0.01$ s^{-1}, $j_0 = 1$, and $M = 100$.

6. Discussion

In this paper, we have extended a model for the unwinding of double-stranded nucleic acids by helicases to allow calculation of helicase processivity. An interaction potential describes how the helicase and NA ss–ds junction affect each other. We assume that the local unbinding rate of the helicase depends exponentially on the interaction potential. The mean attachment time, the translocation processivity, and the unwinding processivity depend on initial conditions: if the position where the helicase binds to the ssNA is varied, the processivity changes. Therefore, in different experimental situations different values of the processivity could be obtained.

A hard-wall interaction potential describes passive unwinding. In this case, the unwinding velocity v_{HW} is significantly slower than the single-strand translocation rate of the motor far from the ss–ds junction. The average attachment time for the hard-wall potential is $\langle\tau\rangle = \gamma^{-1}$ since the unbinding rate γ is independent of position. In other words, the mean attachment time of a passive helicase is the same whether the helicase translocates on ssNA or unwinds dsNA. For initial conditions where the helicase and junction are adjacent to each other, $\langle\delta m\rangle \approx v_{\mathrm{HW}}\langle\tau\rangle$—the translocation processivity is approximately the unwinding velocity times the attachment time. The translocation processivity is lower for a passive helicase during unwinding (relative to ss translocation); this decrease occurs solely because of the decrease in velocity of the helicase, while the average attachment time is unchanged.

We represent active unwinding by a linearly increasing potential of finite range, characterized by the step height U_0 and the number of steps N. A range of up to 10 bases is motivated by the typical size of a helicase monomer. Indeed, structures determined by x-ray diffraction suggest that a helicase can interact with five to ten bases in the ds region of the ss–ds junction [47–53]. We find that for an active helicase the unwinding velocity can approach the single-strand translocation rate of the motor. In other words, the helicase can unwind as fast as it translocates on ssNA.

In contrast to the passive case, the attachment time of an active helicase is shorter during unwinding than during ss translocation. Decreased attachment time during unwinding is a general property of actively opening helicases in our model. Our representation of the unbinding rate assumes that the helicase is bound in a single potential well with a barrier separating the bound state from the unbound state. This model is an approximation, because the helicase exists in different biochemical states throughout the ATP hydrolysis cycle. Each state might experience a different free-energy barrier to unbinding. In principle, if the relative time spent in each of these states changes (for example, as the ATP concentration is varied),

the unbinding rate might vary as well. However, experimental evidence suggests that our simplified model is a good approximation. Single-molecule measurements on RecBCD [13] and UvrD [30] find that the average attachment times of these helicases are independent of ATP concentration. Therefore, the assumption that the potential well for a bound helicase is independent of hydrolysis state is consistent with experiments.

In our model, an actively unwinding helicase shows a decrease in attachment time. Previous work has suggested that high helicase processivity may require two helicase–NA binding sites—one on the ssNA, and another on the dsNA [1, 54, 55]. In this mechanism, a helicase may unbind from the ssNA but remain bound at the dsNA site. The opportunity for dsNA binding is absent when the helicase translocates on ssNA. This effect can be incorporated in our description by introducing an extra binding energy and consequently reduced detachment rate if the helicase is close to the junction.

Both the velocity of unwinding and measures of processivity are sensitive to ΔG, the average free energy of NA base-pair opening. The value of ΔG can be controlled in single-molecule experiments where tension is applied to the ends of the NA, by the concentration of ss-binding proteins in the buffer solution, and by varying the base composition of the NA.

Measurements of helicase velocity and processivity as a function of ΔG can provide information about the interaction between the helicase and the NA ss–ds junction. Because the rate of passive unwinding is determined by the opening probability of the base pair at the junction, the velocity and the processivity decrease rapidly as ΔG increases. For active opening, the unwinding velocity as a function of ΔG depends sensitively on the step height: while for larger values of U_0 the velocity depends only weakly on ΔG, this dependence becomes strong for small U_0. The average attachment time $\langle \tau \rangle$ behaves differently. For a hard-wall interaction potential, the attachment time is independent of ΔG. For active unwinding, the attachment time depends strongly on ΔG for larger U_0 and tends to decrease for increasing ΔG. The effects of ΔG on velocity and attachment time approximately cancel when computing the processivities, so that the behaviour of $\langle \delta m \rangle$ as a function of ΔG is similar for different step heights. Galletto *et al* found that the unwinding rate of DnaB helicase depends on the DNA GC content [56]. Varying the fraction of GC versus AT base pairs changes the average ΔG of the NA template. The dependence on GC content found in these experiments would be expected in our model for an interaction potential with a small (or zero) step height.

For the helicase PcrA, crystal structures suggest that the protein binds both the ss and dsDNA and distorts the double helix [51]. If the protein residues which have been proposed to interact with the dsDNA are mutated, the mutant proteins hydrolyse ATP in the presence of ssDNA at a rate similar to the wild-type protein, but unwind dsDNA 10–30 times more slowly than wild type [57]. In the language of our analysis, the mutations may alter the interaction potential between junction and helicase such that it resembles the passive (hard-wall) case. In our description, changing from a situation of active opening with optimally chosen step height and step number to a passive case with hard-wall potential typically leads to a decrease of the unwinding rate by a factor of $c^{-1} \approx 7$. Further altering the potential to an attractive linear potential [40] with a well depth of $2\,k_{\mathrm{B}}T$ decreases the unwinding rate by a factor of 35. Small changes to the interaction potential can thus cause the unwinding rate to vary by a large factor.

In single-molecule experiments on UvrD helicase, Dessinges *et al* observed the unwinding of DNA molecules by UvrD at different forces [30]. In these experiments, the end-to-end extension of a tethered DNA molecule changes with time as a result of the transformation of dsDNA into ssDNA by the helicase. These single-molecule experiments found that unwinding can be induced by UvrD monomers. However, bulk experiments have suggested that helicase activity requires UvrD dimers [58–60], even though UvrD monomers have a large processivity (2400 bases) when translocating on ssDNA [60]. The reasons for this difference are not

currently understood. The velocity of unwinding was shown by Dessinges *et al* to depend on ATP concentration [30]. In addition, events were observed where the DNA slowly closed at an ATP-dependent rate. It was suggested that these events occur when a UvrD molecule bound near the ss–ds junction switches from one DNA single strand to the other. Because the two single strands have opposite polarity, the helicase might move away from the junction after strand switching. In this interpretation, the re-zipping events provide information on ss translocation of UvrD. The re-zipping velocity would be expected to be greater than or equal to the ss translocation rate of UvrD, because the energetically favourable re-annealing of the two DNA strands behind the helicase might accelerate the protein's motion.

We can relate three key measurements of UvrD motion by Dessinges *et al* [30] to the behaviour of active unwinding discussed here. First, the experiments show that the re-zipping velocity and the unwinding velocity are comparable in certain situations: the re-zipping velocity is approximately 15% larger than the unwinding rate at 35 pN applied force. Second, the effective detachment rate is about ten times larger during unwinding than during re-zipping (at 35 pN). Third, the measured unwinding velocity is only weakly dependent on ΔG. The velocity was measured for 3 and 35 pN applied force on the DNA. The first case corresponds to an increase of ΔG, while in the second case ΔG decreases [30]. If we interpret re-zipping events as approximating the ss translocation behaviour of UvrD, all three of these experimental observations are consistent with our description of an active helicase.

The comparison of these data to bulk measurements reveals agreement in the unbinding rate during ss translocation but not in the unwinding rate. The unbinding rate of UvrD monomers translocating on ssDNA measured in bulk by Fischer *et al* is comparable to (two times larger than) the unbinding rate measured by Dessinges *et al* for UvrD monomers during re-zipping events [60]. Fischer *et al* found that the UvrD unwinding rate was approximately three times slower than the ss translocation rate [60]. However, the bulk experiments of Fischer *et al* observed unwinding only by UvrD dimers, whereas the single-molecule experiments of Dessinges *et al* observed unwinding by UvrD monomers. Therefore the unwinding data may not be directly comparable.

Our physical theory describes how helicase unwinding velocity and processivity depend on the interaction potential between the helicase and the ss–ds junction. This type of theory includes more detail than models based on kinetic states and transitions between them, while neglecting many details present in all-atom simulation models. Physical descriptions of the type we describe here complement other modelling frameworks. Simplifying some aspects of the system—for example, our choice to neglect the biochemical states which occur during helicase ss translocation—allows us to focus on the coupling between helicase translocation and NA unwinding. This level of detail may allow one to relate observed helicase behaviour to simple physical mechanisms, and thereby gain more insight into the parameters which are important for helicase behaviour. For example, experiments on UvrD suggest that this helicase unbinds more rapidly when unwinding dsDNA than during ss translocation [30]. Our model gives a physical picture for why this might happen: an interaction potential corresponding to active opening naturally leads to accelerated helicase unbinding.

Our simple description neglects several effects. We ignore deformations of the NA strand, such as bending and torsion, and treat the strand as a rigid structure. The helicase is described by forward and backward rates only; we neglect the details of the protein's biochemical states. In addition, we ignore the effects of the NA base sequence on opening. These effects are believed to be weak for most helicases [1], although sequence dependence has been demonstrated for Rho [61] and DnaB [56] helicases. Recent work by Kafri, Lubensky and Nelson [62] shows that a motor protein which translocates on a random track can show interesting behaviour near the stall force.

Acknowledgments

We thank D Lubensky, T Perkins, and J Prost for helpful discussions. MDB acknowledges funding from the Council on Research and Creative Work of the University of Colorado.

References

[1] Lohman T M and Bjornson K P 1996 Mechanisms of helicase-catalyzed DNA unwinding *Annu. Rev. Biochem.* **65** 169–214
[2] van Brabant A J, Stan R and Ellis N A 2000 DNA helicases, genomic instability, and human genetic disease *Annu. Rev. Genom. Hum. Genet.* **1** 409–59
[3] von Hippel P H and Delagoutte E 2001 A general model for nucleic acid helicases and their coupling within macromolecular machines *Cell* **104** 177–90
[4] Singleton M R and Wigley D B 2002 Modularity and specialization in superfamily 1 and 2 helicases *J. Bacteriol.* **184** 1819–26
[5] Boehmer P E 1998 The herpes simplex virus type-1 single-strand DNA-binding protein, ICP8, increases the processivity of the UL9 protein DNA helicase *J. Biol. Chem.* **273** 2676–83
[6] Soultanas P, Dillingham M S, Papadopoulos F, Phillips S E V, Thomas C D and Wigley D B 1999 Plasmid replication initiator protein RepD increases the processivity of PcrA DNA helicase *Nucl. Acids Res.* **27** 1421–8
[7] Noirot-Gros M F, Soultanas P, Wigley D B, Ehrlich S D, Noirot P and Petit M A 2002 The beta-propeller protein YxaL increases the processivity of the PcrA helicase *Mol. Genet. Genom.* **267** 391–400
[8] Stano N M, Jeong Y J, Donmez I, Tummalapalli P, Levin M K and Patel S S 2005 DNA synthesis provides the driving force to accelerate DNA unwinding by a helicase *Nature* **435** 370–3
[9] Levin M K, Wang Y H and Patel S S 2004 The functional interaction of the hepatitis C virus helicase molecules is responsible for unwinding processivity *J. Biol. Chem.* **279** 26005–12
[10] Byrd A K and Raney K D 2004 Protein displacement by an assembly of helicase molecules aligned along single-stranded DNA *Nat. Struct. Mol. Biol.* **11** 531–8
[11] Tackett A J, Chen Y F, Cameron C E and Raney K D 2005 Multiple full-length NS3 molecules are required for optimal unwinding of oligonucleotide DNA *in vitro J. Biol. Chem.* **280** 10797–806
[12] Yin H, Artsimovitch I, Landick R and Gelles J 1999 Nonequilibrium mechanism of transcription termination from observations of single RNA polymerase molecules *Proc. Natl Acad. Sci. USA* **96** 13124–9
[13] Bianco P R, Brewer L R, Corzett M, Balhorn R, Yeh Y, Kowalczykowski S C and Baskin R J 2001 Processive translocation and DNA unwinding by individual RecBCD enzyme molecules *Nature* **409** 374–8
[14] Perkins T T, Li H W, Dalal R V, Gelles J and Block S M 2004 Forward and reverse motion of single RecBCD molecules on DNA *Biophys. J.* **86** 1640–8
[15] Lohman T M 1993 Helicase-catalyzed DNA unwinding *J. Biol. Chem.* **268** 2269–72
[16] Delagoutte E and von Hippel P H 2002 Helicase mechanisms and the coupling of helicases within macromolecular machines—part I: structures and properties of isolated helicases *Q. Rev. Biophys.* **35** 431–78
[17] Dohoney K M and Gelles J 2001 Chi-sequence recognition and DNA translocation by single RecBCD helicase/nuclease molecules *Nature* **409** 370–4
[18] Spies M, Bianco P R, Dillingham M S, Handa N, Baskin R J and Kowalczykowski S C 2003 A molecular throttle: the recombination hotspot chi controls DNA translocation by the RecBCD helicase *Cell* **114** 647–54
[19] Handa N, Bianco P R, Baskin R J and Kowalczykowski S C 2005 Direct visualization of RecBCD movement reveals cotranslocation of the RecD motor after chi recognition *Mol. Cell* **17** 745–50
[20] Taylor A F and Smith G R 2003 RecBCD enzyme is a DNA helicase with fast and slow motors of opposite polarity *Nature* **423** 889–93
[21] Dillingham M S, Spies M and Kowalczykowski S C 2003 RecBCD enzyme is a bipolar DNA helicase *Nature* **423** 893–7
[22] Singleton M R, Dillingham M S, Gaudier M, Kowalczykowski S C and Wigley D B 2004 Crystal structure of RecBCD enzyme reveals a machine for processing DNA breaks *Nature* **432** 187–93
[23] Lucius A L, Wong C J and Lohman T M 2004 Fluorescence stopped-flow studies of single turnover kinetics of E-coli RecBCD helicase-catalyzed DNA unwinding *J. Mol. Biol.* **339** 731–50
[24] Lucius A L and Lohman T M 2004 Effects of temperature and ATP on the kinetic mechanism and kinetic step-size for E-coli RecBCD helicase-catalyzed DNA unwinding *J. Mol. Biol.* **339** 751–71
[25] Fischer C J and Lohman T M 2004 ATP-dependent translocation of proteins along single-stranded DNA: models and methods of analysis of pre-steady state kinetics *J. Mol. Biol.* **344** 1265–86

[26] Lucius A L, Vindigni A, Gregorian R, Ali J A, Taylor A F, Smith G R and Lohman T M 2002 DNA unwinding step-size of E-coli RecBCD helicase determined from single turnover chemical quenched-flow kinetic studies *J. Mol. Biol.* **324** 409–28
[27] Ha T, Rasnik I, Cheng W, Babcock H P, Gauss G H, Lohman T M and Chu S 2002 Initiation and re-initiation of DNA unwinding by the Escherichia coli Rep helicase *Nature* **419** 638–41
[28] Rasnik I, Myong S, Cheng W, Lohman T M and Ha T 2004 DNA-binding orientation and domain conformation of the E-coli Rep helicase monomer bound to a partial duplex junction: single-molecule studies of fluorescently labelled enzymes *J. Mol. Biol.* **336** 395–408
[29] Henn A, Medalia O, Shi H P, Steinberg M, Franceschi F and Sagi I 2001 Visualization of unwinding activity of duplex RNA by DbpA, a DEAD box helicase, at single-molecule resolution by atomic force microscopy *Proc. Natl Acad. Sci. USA* **98** 5007–12
[30] Dessinges M N, Lionnet T, Xi X G, Bensimon D and Croquette V 2004 Single-molecule assay reveals strand switching and enhanced processivity of UvrD *Proc. Natl Acad. Sci. USA* **101** 6439–44
[31] Xi J, Zhang Z Q, Zhuang Z H, Yang J S, Spiering M M, Hammes G G and Benkovic S J 2005 Interaction between the T4 helicase loading protein (gp59) and the DNA polymerase (gp43): unlocking of the gp59-gp43-DNA complex to initiate assembly of a fully functional replisome *Biochemistry* **44** 7747–56
[32] Doering C, Ermentrout B and Oster G 1995 Rotary DNA motors *Biophys. J.* **69** 2256–67
[33] Chen Y Z, Mi D, Song H-S and Wang X-J 1997 General random walk model of ATP-driven helicase translocation along DNA *Phys. Rev.* E **56** 919–22
[34] Bhattacharjee S M and Seno F 2003 Helicase on DNA: a phase-coexistence based mechanism *J. Phys. A: Math. Gen.* **36** L181–7
[35] Bhattacharjee S M 2004 Helicase activity on DNA as a propagating front *Europhys. Lett.* **65** 574–80
[36] Cox K, Watson T, Soultanas P and Hirst J D 2003 Molecular dynamics simulations of a helicase *Prot. Struct. Funct. Genet.* **52** 254–62
[37] Levin M K, Gurjar M and Patel S S 2005 A Brownian motor mechanism of translocation and strand separation by hepatitis C virus helicase *Nat. Struct. Mol. Biol.* **12** 429–35
[38] Stukalin E B, Phillips H and Kolomeisky A B 2005 Coupling of two motor proteins: a new motor can move faster *Phys. Rev. Lett.* **94** (23)
[39] Liao J C, Jeong Y J, Kim D E, Patel S S and Oster G 2005 Mechanochemistry of T7 DNA helicase *J. Mol. Biol.* **350** 452–75
[40] Betterton M D and Jülicher F 2003 A motor that makes its own track: helicase unwinding of DNA *Phys. Rev. Lett.* **91** 258103
[41] Betterton M D and Jülicher F 2005 Opening of nucleic-acid double strands by helicases. Active versus passive opening *Phys. Rev.* E **71** 011904
[42] Peskin C S, Odell G M and Oster G F 1993 Cellular motions and thermal fluctuations: the Brownian ratchet *Biophys. J.* **65** 316–24
[43] Hunter A W, Caplow M, Coy D L, Hancock W O, Diez S, Wordeman L and Howard J 2003 The kinesin-related protein MCAK is a microtubule depolymerase that forms an ATP-hydrolyzing complex at microtubule ends *Mol. Cell* **11** 445–57
[44] Bringmann H, Skiniotis G, Spilker A, Kandels-Lewis S, Vernos I and Surrey T 2004 A kinesin-like motor inhibits microtubule dynamic instability *Science* **303** 5663
[45] Klein G A, Kruse K, Cuniberti G and Julicher F 2005 Filament depolymerization by motor molecules *Phys. Rev. Lett.* **94** (10)
[46] Parmeggiani A, Julicher F, Peliti L and Prost J 2001 Detachment of molecular motors under tangential loading *Europhys. Lett.* **56** 603–9
[47] Subramanya H S, Bird L E, Brannigan J A and Wigley D B 1996 Crystal structure of a DExx box DNA helicase *Nature* **384** 379–83
[48] Korolev S, Hsieh J, Gauss G H, Lohman T M and Waksman G 1997 Major domain swiveling revealed by the crystal structures of complexes of E-coli Rep helicase bound to single-stranded DNA and ADP *Cell* **90** 635–47
[49] Kim J L, Morgenstern K A, Griffith J P, Dwyer M D, Thomson J A, Murcko M A, Lin C and Caron P R 1998 Hepatitis C virus NS3 RNA helicase domain with a bound oligonucleotide: the crystal structure provides insights into the mode of unwinding *Structure* **6** 89–100
[50] Korolev S, Yao N H, Lohman T M, Weber P C and Waksman G 1998 Comparisons between the structures of HCV and Rep helicases reveal structural similarities between SF1 and SF2 super-families of helicases *Prot. Sci.* **7** 605–10
[51] Velankar S S, Soultanas P, Dillingham M S, Subramanya H S and Wigley D B 1999 Crystal structures of complexes of PcrA DNA helicase with a DNA substrate indicate an inchworm mechanism *Cell* **97** 75–84

[52] Machius M, Henry L, Palnitkar M and Deisenhofer J 1999 Crystal structure of the DNA nucleotide excision repair enzyme UvrB from Thermus thermophilus *Proc. Natl Acad. Sci. USA* **96** 11717–22
[53] Singleton M R, Sawaya M R, Ellenberger T and Wigley D B 2000 Crystal structure of T7 gene 4 ring helicase indicates a mechanism for sequential hydrolysis of nucleotides *Cell* **101** 589–600
[54] Briggs G S, Mahdi A A, Wen Q and Lloyd R G 2005 DNA binding by the substrate specificity (wedge) domain of RecG helicase suggests a role in processivity *J. Biol. Chem.* **280** 13921–7
[55] Rodriguez I, Lazaro J M, Blanco L, Kamtekar S, Berman A J, Wang J M, Steitz T A, Salas M and de Vega M 2005 A specific subdomain in phi 29 DNA polymerase confers both processivity and strand-displacement capacity *Proc. Natl Acad. Sci. USA* **102** 6407–12
[56] Galletto R, Jezewska M J and Bujalowski W 2004 Unzipping mechanism of the double-stranded DNA unwinding by a hexameric helicase: the effect of the 3′ arm and the stability of the dsDNA on the unwinding activity of the Escherichia coli DnaB helicase *J. Mol. Biol.* **343** 101–14
[57] Soultanas P, Dillingham M S, Wiley P, Webb M R and Wigley D B 2000 Uncoupling DNA translocation and helicase activity in PcrA: direct evidence for an active mechanism *EMBO J.* **19** 3799–810
[58] Maluf N K, Ali J A and Lohman T M 2003 Kinetic mechanism for formation of the active, dimeric UvrD helicase-DNA complex *J. Biol. Chem.* **278** 31930–40
[59] Maluf N K and Lohman T M 2003 Self-association equilibria of Escherichia coli UvrD helicase studied by analytical ultracentrifugation *J. Mol. Biol.* **325** 889–912
[60] Fischer C J, Maluf N K and Lohman T M 2004 Mechanism of ATP-dependent translocation of E. coli UvrD monomers along single-stranded DNA *J. Mol. Biol.* **344** 1287–309
[61] Walmacq C, Rahmouni A R and Boudvillain M 2004 Influence of substrate composition on the helicase activity of transcription termination factor rho: reduced processivity of unwinding of RNA-DNA rho hexamers during hybrid regions *J. Mol. Biol.* **342** 403–20
[62] Kafri Y, Lubensky D K and Nelson D R 2004 Dynamics of molecular motors and polymer translocation with sequence heterogeneity *Biophys. J.* **86** 3373–91